Shigella IpaA Binding to Talin Stimulates Filopodial Capture and Cell Adhesion

Cesar Valencia-Gallardo, Charles Bou-Nader, Daniel-Isui Aguilar-Salvador, Nathalie Carayol, Nicole Quenech'du, Ludovic Pecqueur, Hajeung Park, Marc Fontecave, Tina Izard, Guy Tran van Nhieu

Shigella IpaA binding to talin stimulates filopodial capture and cell adhesion

Cesar Valencia-Gallardo[1,2,3,4], Charles Bou-Nader[5,6], Daniel-Isui Aguilar-Salvador[1,2,3,4], Nathalie Carayol[1,2,3,4], Nicole Quenech'Du[1,2,3,4], Ludovic Pecqueur[5,6], HaJeung Park[7], Marc Fontecave[5,6], Tina Izard[8,] Guy Tran Van Nhieu[1,2,3,4,9*]

[1]Equipe Communication Intercellulaire et Infections Microbiennes, Centre de Recherche Interdisciplinaire en Biologie (CIRB), Collège de France, 75005 Paris, France

[2]Institut National de la Santé et de la Recherche Médicale U1050, 75005 Paris, France

[3]Centre National de la Recherche Scientifique UMR7241, 75005 Paris, France

[4]MEMOLIFE Laboratory of excellence and Paris Science Lettres.

[5]Laboratoire de Chimie des Processus Biologiques, Collège De France, 75005 Paris, France.

[6]Centre National de la Recherche Scientifique UMR8229, 75005 Paris, France

[7]Macromolecular X-ray Crystallography Core, Department of Neuroscience, The Scripps Research Institute, Jupiter, FL 33458.

[8]Cell Adhesion Laboratory, Department of Integrative Structural & Computational Biology, The Scripps Research Institute, Jupiter, FL 33458.

[9] Lead contact:

* Correspondence: E-mail: guy.tran-van-nhieu@college-de-france.fr

Tel: 33-1-44-27-14-89

FAX: 33-1-44-27-14-19

Running title: Talin targeting by an IpaA VBS

Keywords: *Shigella* - IpaA - talin - vinculin - adhesion

Summary

The Shigella type III effector IpaA contains three binding sites for the focal adhesion protein vinculin (VBSs), which are involved in bacterial invasion of host cells. Here, we report that IpaA VBS3 unexpectedly binds to talin. The 2.5 Å resolution crystal structure of IpaA VBS3 in complex with the talin H1-H4 helices shows a tightly folded α-helical bundle, which is in contrast to the bundle unraveling upon vinculin interaction. High-affinity binding to talin H1-H4 requires a core of hydrophobic residues and electrostatic interactions conserved in talin VBS H46. Remarkably, IpaA VBS3 localizes to filopodial distal adhesions enriched in talin, but not vinculin. In addition, IpaA VBS3 binding to talin was required for filopodial adhesions and efficient capture of Shigella. These results point to the functional diversity of VBSs and support a specific role for talin binding by a subset of VBSs in the formation of filopodial adhesions.

Introduction

The cytoskeletal linkers talin and vinculin play important and distinct roles in integrin-mediated cell adhesion (Atherton et al., 2016; Klapholz and Brown, 2017). While vinculin strengthens adhesion and cytoskeletal anchorage, talin is critically required for the formation and maturation of adhesion structures (Lagarrigue et al., 2016; Yan et al., 2015). Talin consists of an amino-terminal FERM domain connected to a large rod domain containing VBSs buried in helical bundles (Calderwood et al., 2013; Lagarrigue et al., 2016; Yan et al., 2015). Upon activation, talin bridges the cytoplasmic tail of the integrin ß1 subunit with actin filaments (Yan et al., 2015). Stretching of the talin molecule due to actomyosin-dependent contractility leads to the unveiling of VBSs buried in helical bundles along the talin rod domain (Yan et al., 2015). Upon exposure, talin VBSs activate vinculin that further tethers actin filaments to adjust adhesion strength in response to substrate stiffness (Gingras et al., 2005; Yan et al., 2015). In vitro measurements on single molecules indicate that unveiling of VBSs in various talin bundles occurs with a defined hierarchy, suggesting different talin activation states.

Bacterial pathogens have evolved remarkable strategies to invade host cells (Dunn and Valdivia, 2010; Pizarro-Cerda et al., 2012). *Shigella*, the causative agent of bacillary dysentery, invades intestinal epithelial cells after being captured by filopodia using a type III secretion system (T3SS) that injects bacterial effectors into host cells (Dunn and Valdivia, 2010; Galan et al., 2014; Valencia-Gallardo et al., 2015). The *Shigella* IpaA type III effector contains three exposed VBSs located within its 145 carboxy-terminal residues that act in concert to promote bacterial invasion (Izard et al., 2006; Park et al., 2011; Tran Van Nhieu and Izard, 2007). Here,

we show that in addition to vinculin, IpaA VBS3 also directly targets talin. IpaA VBS3 forms a folded globular structure with the H1-H4 helices in the talin R1 bundle, which differs from the stretched bundle structure expected during full talin activation. Our results suggest that binding of IpaA VBS3 to a semi-stretched talin conformer stabilizes filopodial adhesions and stimulates bacterial capture.

Results

Talin is recruited by IpaA and is required for *Shigella* invasion

IpaA recruits vinculin at *Shigella* invasion sites to trigger the formation of a transient adhesion required for bacterial internalization by epithelial cells (Tran Van Nhieu et al., 1997). Talin is also recruited at *Shigella* entry sites, but its role requires clarification. When analyzed by immunofluorescence microscopy, talin was detected in coat-structures around internalized bacteria as early as 10 min-incubation at 37°C (Suppl. Figs. 1A, B, arrowhead). Talin recruitment and coalescing around internalized bacteria occurred concomitantly with the depolymerization of actin in membrane ruffles (Figs. 1A, B and Suppl. Figs. 1A, B). Cell treatment with anti-talin siRNA did not impair actin polymerization at *Shigella* invasion sites but actin coat-structures surrounding invading bacteria seldom formed, reminiscent of foci induced by an *ipaA* mutant (Figs. 1A, B). Consistently, bacterial invasion was reduced by 4-fold in anti-talin siRNA-treated cells compared to control cells (Fig. 1C). A *Shigella ipaA* mutant strain failed to form talin coats suggesting a role for IpaA in talin recruitment at invasion sites (Figs. 1D-E, Suppl. Figs. 1C-E).

To investigate the role of IpaA VBSs in the formation of talin coat structures, cells were challenged with *ipaA* mutant strains complemented with IpaA derivatives. Talin coat-structures were not detected for the *ipaA* mutant complemented with vector alone or IpaA deleted for all its VBSs (Figs. 1D, E). Complementation of the *ipaA* mutant with full length IpaA, IpaA ΔVBS1-2 or IpaA ΔVBS3, restored the formation of foci with talin coat structures (Fig. 1E). However, a significant decrease in the percentage of foci forming talin coat structures was observed for the *ipaA* mutant strains expressing IpaA ΔVBS1-2 or IpaA ΔVBS3 compared to full length IpaA, with 19 ± 0.7 % and 25 ± 5 % relative to 52 ± 6.7 %, respectively (Fig. 1E). These results indicate that talin recruitment could occur via IpaA VBS3, or via IpaA VBS1-2 possibly through vinculin-talin interactions.

These results indicate that talin is required for *Shigella* invasion and is recruited at entry sites in an IpaA-dependent manner to form actin coats surrounding invading bacteria.

IpaA VBS3 binds to talin

To confirm and further investigate how IpaA VBS3 recruited talin, we performed a yeast two-hybrid screen using an established human placental cDNA library corresponding to a total of 82.02 million prey clones and a bait containing IpaA1-565 containing the VBS3 but devoid of the VBS1-2 sites (559-633). This screen identified 150 clones representing 16 different genes. Among these, talin was identified with very high confidence in 95 prey clones, with clones corresponding to different open reading frames in talin (Suppl. Table 1). As expected, vinculin was also identified as a prey (Suppl. Table 1). To test whether IpaA VBS3 could directly bind to talin, we performed native gel shift assays using synthetic peptides (Exp. Procedures). As observed for vinculin, IpaA VBS3 did not bind to talin R1 (talin H1-H5), but formed a complex with talin H1-H4 suggesting the targeting of active talin in which the inhibitory H5 helix is removed by mechanical stretching (Papagrigoriou et al., 2004)(Fig. 2A; Suppl. Fig. 4B). In contrast, even at high molar ratios, IpaA VBS1 and IpaA VBS2 did not form any detectable complex with talin H1-H4. ITC measurements indicated that IpaA VBS3 bound to talin H1-H4 with high affinity (K_D = 174 ± 19 nM), whereas IpaA VBS2 did not show any detectable interaction with talin H1-H4 (Fig. 2B; Table 1). IpaA VBS1 interacted with talin H1-H4 with much lower affinity than IpaA VBS3 (K_D = 15.2 ± 1.1 μM; Fig. 2B; Table 1). When native gel shift assays using IpaA 483-633 containing all three VBS1-3 (A483) were performed, a clear migration shift corresponding to a A483-talin H1-H4 complex was observed with depletion of free talin H1-H4 (Fig. 2C, arrowhead). In contrast, when IpaA 524-634 containing only IpaA VBS 1-2 (A524) was incubated with talin H1-H4, no migration shift could be detected (Fig. 2C, A524).

Size-exclusion chromatography coupled with multi-angle static light scattering (SEC-MALS) analysis indicated that A483 and A524 were monomers in solution, as indicated by the molecular mass determination (Fig. 2D; Suppl. Table 2). Of note, H1-H4 behaved as a globular dimer in SEC-MALS analysis (Fig. 2D; Suppl. Table 2), consistent with the crystal structure of talin rod 482-655 (Papagrigoriou et al., 2004). When mixed prior to analysis, only single species corresponding to the talin H1-H4 dimer or A524 monomer were recovered, consistent with the native gels and ITC results (Fig. 2D; Suppl. Table 2). In contrast, a compact globular complex corresponding to one talin H1-H4 dimer bound to a single A483 molecule was

observed (Fig. 2D, talin H1-H4 + A483; Suppl. Table 2). These results are in agreement with the ITC measurements and suggest that A483 strongly interacts with the talin H1-H4 via IpaA VBS3. These results indicate that in addition to vinculin, IpaA VBS3 also binds to talin with high affinity, a property not shared with other IpaA VBSs.

IpaA VBS3 mimics talin H5 to form an α-helix bundle with talin H1-H4

We solved the crystal structure of the IpaA VBS3-talin H1-H4 complex at 2.5 Å resolution (Suppl. Table 3). The complex was purified using a strategy similar to that used for the IpaA VBS3-vD1 complex (Park et al., 2011). The asymmetric unit contains 6 molecules of talin H1-H4 organized into dimers as observed in SEC-MALS (Suppl. Fig. 2). Each talin H1-H4 molecule shows a clear additional density corresponding to the IpaA VBS3 peptide in vicinity of mainly the H2 and H4 helices (Suppl. Fig. 2B). All talin H1-H4 chains in the asymmetric unit were very similar with pairwise RMSDs in the range 0.28-0.64 Å over 140 Cα. The interface area between IpaA VBS3 and talin H1-H4 is 849 ± 26 $Å^2$ and involves mainly hydrophobic residues located in talin α-helices H2, H3 and H4 (Figs. 3A, B). In addition, electrostatic interactions, either direct, between K498 and E621, or indirect with R489 pointing within a negatively charged region, further strengthen IpaA VBS3 binding and positioning in the talin H2-H4 groove (Figs. 3A, B). Structural comparison of IpaA VBS3 in its talin-bound and vinculin-bound state (PDB 3rf3, Fig. 3B) indicates that the same IpaA VBS3 hydrophobic residues are involved in binding to talin H1-H4 and vD1. The IpaA VBS3-vinculin vD1 interaction surface area, however, is wider (1150 $Å^2$) than that of IpaA VBS3-talin H1-H4 and comprises IpaA residues F493, K497 and E490, which are not involved in talin H1-H4 recognition (Fig. 3B). Strikingly, IpaA K498 specifically interacts with talin E621 and does not establish interaction with vD1 (Fig. 3B).

Structural comparison with talin H1-H5 (Figs. 3C-E) reveals a remarkable superposition of VBS3 with H5. I492, A495, V499, L506 and I507 of IpaA VBS3 involved in hydrophobic interaction with talin H1-H4 are homologous to L637, A640, V644, L651 and L652 in the talin α-helix H5, nesting in the identical hydrophobic groove (Figs. 3C-E). Furthermore, a strong similarity in polarity is observed between talin H5 and IpaA VBS3, with IpaA R489 corresponding to talin R634 engaged in the same polar interaction with the talin H2-H3 loop.

Contact residues in IpaA VBS3 determining binding specificity for talin

Synthetic peptides were generated to confirm the role of IpaA polar and hydrophobic residues in talin H1-H4 binding. Specifically, we tested the effects of charge at R489 and K498, and substitution of A495 rationalized by the structural alignment with IpaA and talin VBSs (Suppl. Fig. 3). ITC analysis indicated that the K498A substitution did not significantly decrease the talin-binding affinity of IpaA VBS3, possibly because of the complementary charge contribution by adjacent K497 (Table 1). The single charge inversion K498E, however, led to a 1.7-fold increase in the determined K_D (K_D = 300 ± 2.8 nM) for talin H1-H4. A similar increase was observed for the charge suppressing double mutations R489A K498A with a K_D = 328 ± 1.9 nM. Consistent with a critical role for the hydrophobic interactions, the A495K substitution led to a drastic defect in IpaA VBS3 binding to talin, with a 17-fold increase in K_D (K_D = 2.93 ± 0.3 μM) (Table 1). These results were further confirmed in native gel shift experiments showing that as opposed to IpaA VBS3, IpaA VBS3 498E and IpaA VBS3 A495K did not induce any detectable shift of talin H1-H4 (Suppl. Fig. 4). In contrast, shifts were still observed in the presence of vD1, indicating that the mutations did not prevent complex formation with vinculin, although higher peptide concentrations were required for the A495K substitution consistent with a partial effect of this substitution on vinculin binding (Suppl. Fig. 4B).

Talin-binding by IpaA VBS3 stimulates the formation of nascent adhesions

Our evidence suggests that IpaA VBS3 targets an active conformer of talin containing a 4-helix folded R1 bundle that differs from the "opened" configuration reported to interact with vinculin (del Rio et al., 2009; Papagrigoriou et al., 2004). To test the targeting of a specific talin conformer by IpaA VBS3, we took advantage of its high affinities for vinculin and talin and generated a GFP fusion as a probe to analyze its localization following cell transfection. As shown in Suppl. Fig. 5A, GFP-IpaA VBS3 labeled FAs of cells plated onto fibronectin-coated glass coverslips, showing a strict co-localization with talin and vinculin. As expected, siRNA-mediated depletion experiments showed that GFP-IpaA VBS3 labeling of adhesion structures was vinculin- and talin-dependent (Suppl. Fig. 5). When cells were plated on 15 kPa stiffness substrate, GFP-IpaA VBS3 labeled vinculin and talin-containing adhesions at the cell periphery, including at the base of filopodia as well as at the edge of lamellae. Adhesion structures located towards the cell interior, however, were less enriched in IpaA VBS3, consistent with labeling of nascent adhesions (Suppl. Figs. 5E, F) (Beningo et al., 2001; van Hoorn et al., 2014).

In replating experiments, GFP-IpaA VBS3 labeled talin and vinculin-containing peripheral adhesions, consistent with nascent adhesions, as well as prominent adhesions (Fig. 4A-C). As expected, control cells transfected with GFP alone showed a diffuse cytoplasmic labeling and virtually no recruitment in adhesion structures (Figs. 4B, C). When cells were transfected with the mutated IpaA VBS3 variants, a 6- and 7.8-fold reduction in the number of GFP-IpaA VBS3-positive adhesions per cell were observed for IpaA VBS3 A495K and K498E, respectively, compared to parental IpaA-VBS3 (Figs. 4A-C). In addition, the size of adhesions was significantly reduced in GFP-IpaA VBS3 A495K and K498E transfected cells compared to GFP-IpaA VBS3 transfectants (Figs. 4D, E). Of note, while showing reduced stimulatory effects on adhesion formation, the talin-binding deficient variants A495K and K498E showed an increase in the size of focal adhesions compared to GFP-transfected control cells, with a median ± MAD of 1.53 ± 0.51 and 1.21 ± 0.39, respectively (Figs. 4D, E), likely due to their residual vinculin-binding ability.

IpaA VBS3 regulates filopodial extension through its talin- but not vinculin-binding activity

In replating experiments, talin was also enriched in adhesions in the filopodial shaft distal moiety while vinculin preferentially localized at the filopodial shaft proximal moiety and base (Fig. 5A), with a median distance ± MAD of 2.5 ± 1.8 μm and 1.7 ± 1.3 μm, respectively (Fig. 5B; Exp. Proc.). In addition, GFP-IpaA VBS3 was associated with distal filopodial talin adhesions, whereas association with vinculin was observed in more proximal filopodial adhesions, with a median distance of 2.8 ± 1.5 μm compared to 1.4 ± 0.9 μm, respectively (Fig. 5C; Suppl. Fig. 6). VBS3- and talin-labeled adhesions were located more distally than talin- and vinculin-labeled adhesions in filopodia, suggesting the formation of distinct complexes (Fig. 5C). Consistent with different talin conformers, the canonical talin-binding domain of vinculin vD1 labeled filopodial clusters that were more proximal to the cell body than those labeled with VBS3, with a median distance to the cell body of 2.5 ± 1.8 μm and 3.1 ± 2.2 μm, respectively (Fig. 5D). As expected, GFP alone did not label structures in filopodia (Fig. 5E; Suppl. Fig. 6).

To test the role of talin-binding in the targeting of filopodial distal adhesions by IpaA VBS3, we analyzed the localization of the GFP-IpaA VBS3 A495K and K498E mutants. As opposed to GFP-IpaA VBS3, the mutated VBS3 variants impaired for talin binding showed a 2.7-fold decrease labeling of large filopodial adhesions (Figs. 5A, E). Binding of vD1 to activated talin

was shown to inhibit its refolding, thereby stabilizing focal adhesions (Atherton et al., 2015; Yao et al., 2014). We therefore expected binding of IpaA VBS3 to favor filopodial extension by stabilizing filopodial adhesions. Consistently, quantification indicated that filopodia in GFP-IpaA VBS3 transfectants were longer than those observed in cells transfected with GFP-talin with a median length ± MAD of 4.1 ± 1.9 μm and 3.4 ± 1.9 μm, respectively (Fig. 5F). Remarkably, cells transfected with GFP-IpaA VBS3 A495K and K498E showed filopodia that were significantly shorter than cells transfected with GFP-IpaA VBS3 with a median length of 2.6 ± 0.8 μm and 2.9 ± 1 μm, respectively, and comparable to the filopodial length in cells transfected with vD1 (Fig. 5F, median 2.5 ± 1.8 μm). In control experiments, the filopodial length in cells co-transfected with GFP and mCherry-talin or vinculin-mCherry were comparable to those of GFP-talin alone or GFP-VBS3 K498E, with a median length of 3.0 ± 1.1 and 2.9 ± 0.1 μm, respectively (Fig. 5F).

Together, these results suggest that through talin binding, IpaA VBS3 stabilizes filopodial adhesions thereby favoring their extension. The role of IpaA VBS3 in the regulation of both filopodial and nascent adhesions further supports the link reported between these adhesion structures (Hoffmann and Schafer, 2010; Jacquemet et al., 2015; Partridge and Marcantonio, 2006).

Talin binding by IpaA VBS3 stimulates filopodial capture and *Shigella*-induced cell adhesion formation

Shigella invasion of epithelial cells is preceded by its capture by filopodia (Romero et al., 2011). We next analyzed the effects of GFP-IpaA VBS3 transfection in bacterial capture (Romero et al., 2011). As shown in Fig. 6A, GFP-IpaA VBS3 and talin structures could be observed at the tip of 84.6 % of filopodia capturing bacteria (Fig. 6A, arrowhead; 13 filopodia, N = 3), but only in 12.8 % of filopodia devoid of bacteria (304 filopodia, N = 3). To test the relevance of talin-binding by IpaA VBS3 during filopodial capture, cells were challenged with *ipaA* mutant strains complemented with various IpaA constructs. As shown in Fig. 6B, deletion of all IpaA VBSs resulted in a five-fold reduction in the number of bacterial capture compared to full-length IpaA. While deletion of IpaA VBS1-2 containing VBS3 did not affect filopodial capture, deletion of IpaA VBS3 reduced filopodial capture by 2.4-fold (Fig. 6B). The A495K or K498E mutations that impaired talin binding reduced filopodial capture to similar extent than IpaA ΔVBS3 (Fig. 6B).

In addition to forming pseudo-adhesion structures in membrane ruffles during invasion, *Shigella* stabilizes FAs to prevent early detachment of infected cells (Sun et al., 2017). To investigate the role of IpaA VBS3 in this process, cells were challenged with bacteria for 30 min and talin-containing adhesions were analyzed by immunofluorescence microscopy (Exp. Procedures). As shown in Figs. 6C,D, while showing less focal adhesions than uninfected cells, cells infected with the *ipaA* mutant complemented with full length IpaA remained spread and showed large adhesion structures. In contrast, cells challenged with *ipaA* mutant complemented with vector alone showed a significant decrease in size and number of adhesions (Figs. 6C-D). Complementation with IpaA ΔVBS1-2 containing VBS3 restored adhesion structures although these latter were smaller than those observed for full-length IpaA (Figs. 6C, D). Strikingly, the A495K and K498E mutations affected the IpaA VBS3-dependent formation of adhesion structures at different degrees. Cells infected with *ipaA* / IpaA ΔVBS1-2-A495K were similar to cells infected with *ipaA* complemented with vector alone, with smaller and fewer adhesion structures compared to *ipaA* / IpaA ΔVBS1-2 (Figs. 6C-D). Complementation with IpaA ΔVBS1-2-K498E led to an intermediate phenotype with similar numbers of adhesions per cell but a clear shift in the distribution towards cells showing smaller adhesions (Figs. 6C-F).

Together, these results indicate that talin binding by IpaA VBS3 plays an important role in bacterial capture by filopodia and stabilizes cell adhesions during *Shigella* infection.

Discussion

Our work provides a mechanistic basis for how IpaA VBS3 acts as a dual talin-vinculin binder, a property not shared by IpaA VBS1 or IpaA VBS2. IpaA residues V499-L503-L507 are involved in interactions with talin or vinculin, suggesting that these constitute a common hydrophobic core essential for binding but not conferring specificity. Two other hydrophobic residues, IpaA I492-A495, however, appear to be specific for talin interaction. Also, electrostatic interactions involving residues IpaA R489 and K498 are important for talin specificity. Specifically, the lysine residue at position 498 in IpaA VBS3 is critical for specific and high affinity binding to talin. The sequence alignment of IpaA and talin VBSs and ITC-based affinity measurements highlight that among the VBSs analyzed, only talin H46 share properties similar to IpaA VBS3 in binding to talin H1-H4 (Table 1, Suppl. Fig. 3). These findings indicate functional diversity between VBSs, with IpaA VBS3 and talin H46 acting as dual vinculin- and talin-binding sites. While this was not investigated in the current study, IpaA

VBS3 may also bind to talin 2, a talin 1 related protein that presents conserved structural features in the R1 bundle (Suppl. Fig. 7).

Our structural and cell labeling data suggest that IpaA VBS3 targets an active talin conformer presenting a folded R1 bundle in filopodial distal adhesions that differs from fully active talin. Stretching experiments on purified talin bundles failed to detect intermediate steps during R1 unfolding (Yao et al., 2014; Yao et al., 2016). Current magnetic tweezers resolution limits, however, do not enable to detect displacement of a single helix, such as that of H5 expected to occur during IpaA VBS3 binding to R1. Recent single molecule atomic force microscopy combined with steered molecular dynamics (SMDs), however, supported the existence of 3-helix intermediates during unfolding of the talin R9 and R11 5-helix bundles (Mykuliak et al., 2018). SMDs also predict that stronger hydrogen and salt bridges interactions between the talin H1 and H4 helices result in a torque leading to dissociation of talin H5 from H4 under applied force (Hytonen and Vogel, 2008; Lee et al., 2007), consistent with a talin conformer with a partially unfolded R1 bundle. Because of their structure, the talin R2 and R3 bundles are proposed to unfold first in response to stretching forces, leading to RIAM dissociation and vinculin binding (Goult et al., 2013b), while R1 and R10 unfold at intermediate forces (del Rio et al., 2009; Wang and Ha, 2013; Yao et al., 2014; Yao et al., 2016). Talin VBSs' exposure in cells, however, may be altered by ligands stabilizing talin bundles or in the talin auto-inhibited state (Goult et al., 2013a).

Early studies had pointed to a role for talin in controlling filopodial elongation and retraction (Sydor et al., 1996). In line with this, the functional analysis of mutated IpaA VBS3 indicated that talin-binding is specifically required for filopodial adhesions and bacterial capture. Consistently, IpaA A495K and K498E mutations that decrease talin-binding activity prevented the localization of IpaA VBS3 in filopodial shaft adhesions and its effects on filopodia elongation. We propose that in crawling filopodia, IpaA VBS3 favors filopodial protrusion by stabilizing talin-mediated cytoskeletal anchorage at filopodial shaft adhesions. Talin contains a C-terminal F-actin-binding domain involved in talin dimer formation (Gingras et al., 2008). It is possible that talin-talin interactions are favored during initial activation steps. Interactions between talin H1-H4 and IpaA VBS3 or talin H46 may stabilize and / or contribute to the formation of higher order talin oligomers devoid of vinculin in filopodial tip and distal adhesions, acting as a molecular clutch adapted to the low force range exerted by filopodia.

Adhesions involving this talin-based clutch would serve as anchoring points favoring filopodial extension through actin polymerization at the tip of filopodia.

Unlike talin VBSs, IpaA VBSs are not buried within bundles and may bind to available ligands in an opportunistic manner. Following capture by swirling filopodia, IpaA VBS3 may bind to talin R1 to stabilize the filopodial tip adhesion. Because pathogens often mimic cellular processes, a similar role may be performed by talin H46 in the R10 bundle during filopodial sensing. Upon filopodial retraction IpaA VBS3 may cooperate with IpaA VBS1-2 to trigger vinculin activation and reinforce cytoskeletal tethering. IpaA could possibly also bridge activated vinculin through its VBS1, 2 and talin trough its VBS3, thereby contributing in the cross-linking of cytoskeletal network at *Shigella* invasion sites. As force increases, further stretching of talin will lead to the dissociation of VBS3- talin recipient bundle interaction and subsequent VBS-vinculin interaction, in line with the enrichment of vinculin at proximal filopodial shaft and basal adhesions.

Acknowledgments

The authors thank Dr. Olivera Francetic for careful reading of the manuscript and Dr. David Stroebel (IBENS) for his help with ITC measurements. This work benefited from the facilities of the *Plateforme de Mesures d'Interaction des Macromolécules* (PIM), I2BC (http://www.cgm.cnrs-gif.fr/) and from the *Plateforme de Proteomique (Ecole Normale Superieure)*. We acknowledge SOLEIL for provision of synchrotron radiation facilities (proposal ID 20150780) and we would like to thank Proxima 1 team for assistance in using the beamline. This work was supported by grants from the Inserm, the CNRS and the Collège de France to the CIRB, as well as grant from the PSL Idex project "Shigaforce". CV-G is a recipient of a PhD fellowship from the Memolife Labex and a post-doctoral fellowship from the PSL Idex. NC is a recipient of an IRG Marie-Curie fellowship. DA is funded by CONACYT and the Labex Memolife international PhD program.

Author contributions

NC, NQ-D, LP, HJ P performed and analyzed experiments. MF, and TI analyzed experiments. C V-G, C B-N, DIAS, and GTVN performed, analyzed experiments and wrote the manuscript.

Conflict of interest

The authors declare no conflict of interest.

References

Atherton, P., B. Stutchbury, D. Jethwa, and C. Ballestrem. 2016. Mechanosensitive components of integrin adhesions: Role of vinculin. *Exp Cell Res*. 343:21-27.

Atherton, P., B. Stutchbury, D.Y. Wang, D. Jethwa, R. Tsang, E. Meiler-Rodriguez, P. Wang, N. Bate, R. Zent, I.L. Barsukov, B.T. Goult, D.R. Critchley, and C. Ballestrem. 2015. Vinculin controls talin engagement with the actomyosin machinery. *Nat Commun*. 6:10038.

Beningo, K.A., M. Dembo, I. Kaverina, J.V. Small, and Y.L. Wang. 2001. Nascent focal adhesions are responsible for the generation of strong propulsive forces in migrating fibroblasts. *J Cell Biol*. 153:881-888.

Borgon, R.A., C. Vonrhein, G. Bricogne, P.R. Bois, and T. Izard. 2004. Crystal structure of human vinculin. *Structure*. 12:1189-1197.

Bricogne, G., E. Blanc, M. Brandl, C. Flensburg, P. Keller, P. Paciorek, P. Roversi, A. Sharff, O.S. Smart, C. Vonrhein, and T.O. Womack. 2011. BUSTER version 2.9. . *Global Phasing Ltd., Cambridge, UK. https:// www.globalphasing.com/buster/*. .

Calderwood, D.A., I.D. Campbell, and D.R. Critchley. 2013. Talins and kindlins: partners in integrin-mediated adhesion. *Nat Rev Mol Cell Biol*. 14:503-517.

de Chaumont, F., S. Dallongeville, N. Chenouard, N. Herve, S. Pop, T. Provoost, V. Meas-Yedid, P. Pankajakshan, T. Lecomte, Y. Le Montagner, T. Lagache, A. Dufour, and J.C. Olivo-Marin. 2012. Icy: an open bioimage informatics platform for extended reproducible research. *Nat Methods*. 9:690-696.

del Rio, A., R. Perez-Jimenez, R. Liu, P. Roca-Cusachs, J.M. Fernandez, and M.P. Sheetz. 2009. Stretching single talin rod molecules activates vinculin binding. *Science*. 323:638-641.

Dunn, J.D., and R.H. Valdivia. 2010. Uncivil engineers: Chlamydia, Salmonella and Shigella alter cytoskeleton architecture to invade epithelial cells. *Future Microbiol*. 5:1219-1232.

Emsley P, Lohkamp B, Scott WG, Cowtan K. 2010. Features and development of Coot. Acta Crystallogr D Biol Crystallogr. 66(Pt 4):486-501.

Galan, J.E., M. Lara-Tejero, T.C. Marlovits, and S. Wagner. 2014. Bacterial type III secretion systems: specialized nanomachines for protein delivery into target cells. *Annu Rev Microbiol*. 68:415-438.

Gingras, A.R., N. Bate, B.T. Goult, L. Hazelwood, I. Canestrelli, J.G. Grossmann, H. Liu, N.S. Putz, G.C. Roberts, N. Volkmann, D. Hanein, I.L. Barsukov, and D.R. Critchley. 2008. The structure of the C-terminal actin-binding domain of talin. *EMBO J*. 27:458-469.

Gingras, A.R., W.H. Ziegler, R. Frank, I.L. Barsukov, G.C. Roberts, D.R. Critchley, and J. Emsley. 2005. Mapping and consensus sequence identification for multiple vinculin binding sites within the talin rod. *J Biol Chem*. 280:37217-37224.

Goult, B.T., X.P. Xu, A.R. Gingras, M. Swift, B. Patel, N. Bate, P.M. Kopp, I.L. Barsukov, D.R. Critchley, N. Volkmann, and D. Hanein. 2013a. Structural studies on full-length talin1 reveal a compact auto-inhibited dimer: implications for talin activation. *J Struct Biol*. 184:21-32.

Goult, B.T., T. Zacharchenko, N. Bate, R. Tsang, F. Hey, A.R. Gingras, P.R. Elliott, G.C. Roberts, C. Ballestrem, D.R. Critchley, and I.L. Barsukov. 2013b. RIAM and vinculin binding to talin are mutually exclusive and regulate adhesion assembly and turnover. *J Biol Chem*. 288:8238-8249.

Hoffmann, B., and C. Schafer. 2010. Filopodial focal complexes direct adhesion and force generation towards filopodia outgrowth. *Cell Adh Migr*. 4:190-193.

Hytonen, V.P., and V. Vogel. 2008. How force might activate talin's vinculin binding sites: SMD reveals a structural mechanism. *PLoS Comput Biol*. 4:e24.

Izard, T., G. Tran Van Nhieu, and P.R. Bois. 2006. Shigella applies molecular mimicry to subvert vinculin and invade host cells. *J Cell Biol*. 175:465-475.

Izard, T., and C. Vonrhein. 2004. Structural basis for amplifying vinculin activation by talin. *J Biol Chem*. 279:27667-27678.

Jacquemet, G., H. Hamidi, and J. Ivaska. 2015. Filopodia in cell adhesion, 3D migration and cancer cell invasion. *Curr Opin Cell Biol*. 36:23-31.

Kabsch W. 2010. XDS. Acta Crystallogr D Biol Crystallogr. 66 (Pt 2):125-32.
Klapholz, B., and N.H. Brown. 2017. Talin - the master of integrin adhesions. *J Cell Sci*. 130:2435-2446.
Lagarrigue, F., C. Kim, and M.H. Ginsberg. 2016. The Rap1-RIAM-talin axis of integrin activation and blood cell function. *Blood*. 128:479-487.
Lee, S.E., R.D. Kamm, and M.R. Mofrad. 2007. Force-induced activation of talin and its possible role in focal adhesion mechanotransduction. *J Biomech*. 40:2096-2106.
McCoy AJ, Grosse-Kunstleve RW, Adams PD, Winn MD, Storoni LC, Read RJ. 2007. Phaser crystallographic software. J Appl Crystallogr. 40(Pt 4):658-674.
Mykuliak, V.V., A.W.M. Haining, M. von Essen, A. Del Rio Hernandez, and V.P. Hytonen. 2018. Mechanical unfolding reveals stable 3-helix intermediates in talin and alpha-catenin. *PLoS Comput Biol*. 14:e1006126.
Papagrigoriou, E., A.R. Gingras, I.L. Barsukov, N. Bate, I.J. Fillingham, B. Patel, R. Frank, W.H. Ziegler, G.C. Roberts, D.R. Critchley, and J. Emsley. 2004. Activation of a vinculin-binding site in the talin rod involves rearrangement of a five-helix bundle. *EMBO J*. 23:2942-2951.
Park, H., C. Valencia-Gallardo, A. Sharff, G. Tran Van Nhieu, and T. Izard. 2011. Novel vinculin binding site of the IpaA invasin of Shigella. *J Biol Chem*. 286:23214-23221.
Partridge, M.A., and E.E. Marcantonio. 2006. Initiation of attachment and generation of mature focal adhesions by integrin-containing filopodia in cell spreading. *Mol Biol Cell*. 17:4237-4248.
Pizarro-Cerda, J., A. Kuhbacher, and P. Cossart. 2012. Entry of Listeria monocytogenes in mammalian epithelial cells: an updated view. *Cold Spring Harb Perspect Med*. 2.
Ramarao, N., C. Le Clainche, T. Izard, R. Bourdet-Sicard, E. Ageron, P.J. Sansonetti, M.F. Carlier, and G. Tran Van Nhieu. 2007. Capping of actin filaments by vinculin activated by the Shigella IpaA carboxyl-terminal domain. *FEBS Lett*. 581:853-857.
Romero, S., G. Grompone, N. Carayol, J. Mounier, S. Guadagnini, M.C. Prevost, P.J. Sansonetti, and G.Tran Van Nhieu. 2011. ATP-mediated Erk1/2 activation stimulates bacterial capture by filopodia, which precedes Shigella invasion of epithelial cells. *Cell Host Microbe*. 9:508-519.
Romero, S., A. Quatela, T. Bornschlogl, S. Guadagnini, P. Bassereau, and G. Tran Van Nhieu. 2012. Filopodium retraction is controlled by adhesion to its tip. *J Cell Sci*. 125:4999-5004.
Schagger, H., W.A. Cramer, and G. von Jagow. 1994. Analysis of molecular masses and oligomeric states of protein complexes by blue native electrophoresis and isolation of membrane protein complexes by two-dimensional native electrophoresis. *Anal Biochem*. 217:220-230.
Sun, C.H., B. Wacquier, D.I. Aguilar, N. Carayol, K. Denis, S. Boucherie, C. Valencia-Gallardo, C. Simsek, C. Erneux, A. Lehman, J. Enninga, L. Arbibe, P. Sansonetti, G. Dupont, L. Combettes, and G. Tran Van Nhieu. 2017. The Shigella type III effector IpgD recodes Ca(2+) signals during invasion of epithelial cells. *EMBO J*. 36:2567-2580.
Sydor, A.M., A.L. Su, F.S. Wang, A. Xu, and D.G. Jay. 1996. Talin and vinculin play distinct roles in filopodial motility in the neuronal growth cone. *J Cell Biol*. 134:1197-1207.
Tran Van Nhieu, G., A. Ben-Ze'ev, and P.J. Sansonetti. 1997. Modulation of bacterial entry into epithelial cells by association between vinculin and the Shigella IpaA invasin. *EMBO J*. 16:2717-2729.
Tran Van Nhieu, G., and T. Izard. 2007. Vinculin binding in its closed conformation by a helix addition mechanism. *EMBO J*. 26:4588-4596.
Valencia-Gallardo, C.M., N. Carayol, and G. Tran Van Nhieu. 2015. Cytoskeletal mechanics during Shigella invasion and dissemination in epithelial cells. *Cell Microbiol*. 17:174-182.
van Hoorn, H., R. Harkes, E.M. Spiesz, C. Storm, D. van Noort, B. Ladoux, and T. Schmidt. 2014. The nanoscale architecture of force-bearing focal adhesions. *Nano Lett*. 14:4257-4262.
Wang, X., and T. Ha. 2013. Defining single molecular forces required to activate integrin and notch signaling. *Science*. 340:991-994.
Yan, J., M. Yao, B.T. Goult, and M.P. Sheetz. 2015. Talin Dependent Mechanosensitivity of Cell Focal Adhesions. *Cell Mol Bioeng*. 8:151-159.

Yao, M., B.T. Goult, H. Chen, P. Cong, M.P. Sheetz, and J. Yan. 2014. Mechanical activation of vinculin binding to talin locks talin in an unfolded conformation. *Sci Rep*. 4:4610.
Yao, M., B.T. Goult, B. Klapholz, X. Hu, C.P. Toseland, Y. Guo, P. Cong, M.P. Sheetz, and J. Yan. 2016. The mechanical response of talin. *Nat Commun*. 7:11966.
Yogesha, S.D., E.S. Rangarajan, C. Vonrhein, G. Bricogne, and T. Izard. 2012. Crystal structure of vinculin in complex with vinculin binding site 50 (VBS50), the integrin binding site 2 (IBS2) of talin. *Protein Sci*. 21:583-588.

Figures legends

Fig. 1. Talin is required for *Shigella* invasion and is recruited in an IpaA-dependent manner.

(A) Representative micrographs of control cells and cells treated with anti-talin siRNA prior to bacterial challenge at 37°C for 15 min. Green: actin; red: bacterial LPS. The arrows point to actin "cups" at bacterial cell contact (CTRL) or at the periphery of the foci (siRNA talin). Scale bar = 2 μm.

(B) The average intensity of actin foci was determined at the indicated time points following bacterial challenge for control cells (empty squares) or anti-talin siRNA treated cells (black squares). N = 3, > 30 foci.

(C) Cells were treated with anti-talin siRNA prior to bacterial challenge at 37°C for 15 min. The percentage of internalized bacteria after 30 minutes of infection with WT *Shigella* was determined (Methods). For each samples, n > 35 foci in at least three independent. Wilcoxon test. ****: $p < 0.001$.

(D) Representative micrographs of cells were transfected with talin-GFP and challenged with *Shigella* strains for 30 min at 37°C. Red: bacterial; blue: actin; green: talin-GFP. Cells challenged with the *ipaA* mutant strain complemented with full length IpaA (Bricogne et al.), vector alone (2.1), IpaA ΔVBS3 and IpaA ΔVBS1-2. The arrows point to talin coat structures surrounding invading bacteria. Scale bar = 5 μm.

(E) Average percentage of actin foci forming talin-coat structures induced by the indicated bacterial strain ± SD (Methods). For each sample, n > 35 foci in at least three independent experiments. Chi Squared Test χ^2 with post-hoc comparison (FDR correction for p-value).

Figure 2 – IpaA VBS3 interacts with talin.

(A) Analysis of IpaA VBSs and talin H1-H4 interaction using 6-18 % gradient native PAGE. The talin H1-H4: IpaA VBS molar ratio is indicated with 1 corresponding to a final concentration of 25 μM. Arrowheads point to talin H1-H4 and talin H1-H4:IpaA VBS3.

(B) Isothermal titration calorimetry (ITC) analysis of the interaction between talin H1-H4 and the indicated IpaA VBSs. The estimated K_D are indicated. IpaA VBS2 showed no binding to talin.

(C) Native PAGE analysis. The talin H1-H4: IpaA derivative molar ratios are indicated with 1 corresponding to a final concentration of 25 μM.

(D) SEC-MALS analysis. Indicated proteins were incubated for 60 min in column buffer prior to SEC analysis using a Superdex 200 10/300 GL increase column. Traces: normalized absorbance at 280 nm of the indicated proteins or complex species in the corresponding color. Dotted lines: molecular mass of the indicated proteins or complexes determined by MALS in the corresponding colors.

Figure 3 – IpaA VBS3 forms a compact fold with talin H1-H4

(A) X-ray structure of the talin H1-H4:IpaA VBS3 complex. Blue: talin polypeptide chain. White: interacting residues. Green: bound IpaA VBS3 with interacting residues in green. VBS3 residues are annotated according to full length IpaA.

(B) Molecular detail of the interaction between IpaA VBS3 with talin H1-H4 and vD1. Top panels: IpaA VBS3 is shown in cartoon with its relevant interacting residues. Bottom panels: Talin H1-H4 and vinculin D1 are illustrated by their vacuum electrostatic potential generated with APBS [38]. Of note, the aminoterminal residues Thr 489 to Thr 487 of IpaA VBS3 form an additional helical turn when bound to talin H1-H4 as opposed to the vD1 complex, suggesting that this different fold further tunes recognition specificity.

(C) Superimposition of talin H1-H4:IpaA VBS3 and talin H1-H5 structures. Talin H1-H4 bound to IpaA VBS3 (green) and to talin H5 (pink) are shown as a cartoon in blue and magenta, respectively.

(D) Helical wheel analysis of IpaA VBS3 (top) and talin H5 (bottom) indicates that both are amphipathic α-helices with conserved residues in their hydrophobic interphase. The hydrophobic residues, polar residues, positively and negatively charged residues are colored yellow, green, blue, and red, respectively.

(E) Comparison of talin H1-H4 binding to IpaA VBS3 and talin H5. Talin H1-H4 is shown in white cylinder while the electrostatic surface of IpaA VBS3 and H5 are represented as calculated with APBS.

Fig. 4. Talin-binding by IpaA VBS3 promotes focal adhesions formation.

Cells were trypsinized and replated onto fibronectin-coated glass coverslip for 15 min prior to fixation and processing for fluorescence staining. Samples were analyzed by spinning disk microscopy. Cells transfected with: GFP: GFP-IpaA VBS3 (VBS3), A495K, or K498E variant and talin-mCherry (talin) or mCherry-vinculin (vinculin).

(A) Representative fluorescence micrographs of confocal basal planes. Scale bar = 5 μm.

(B) Wavelet Spot Detection (green) of adhesion structures in replated cells (Exp. Procedures).

(C) Distribution of cells as a function of the number of detected VBS3-labeled adhesions. Median ± MAD: VBS3: 23 ± 10.5 (18 cells, N=3); A495K: 2.5 ± 2.5 (14 cells, N=3); K498E: 1 ± 1 (17 cells, N=3); GFP; 0 ± 0 (9 cells, N=3) Dunn's test. ***: $p < 0.005$. ****: $p < 0.001$.

(D) Size distribution of FAs for talin-mCherry transfected cells. Median ± MAD: VBS3: 1.79 ± 0.76 (774 FAs, N=3); A495K: 1.53 ± 0.51 (568 FAs, N=3); K498E: 1.53 ± 0.51 (383 FAs, N=3); GFP: 1.29 ± 0.39 (878 FAs, N=3). Dunn's test. ***: $p < 0.005$. ****: $p < 0.001$.

(E) Size distribution of FAs for mCherry-vinculin transfected cells. Median ± MAD: VBS3: 2.04 ± 0.76 (629 FAs, N=3); A495K: 1.79 ± 0.76 (595 FAs, N=3); K498E: 1.53 ± 0.51 (480 FAs, N=3); GFP: 1.23 ± 0.32 (482 FAs, N=3). Dunn's test.. ****: $p < 0.001$.

Fig. 5. IpaA VBS3 targets talin-containing filopodial adhesions

Cells transfected with vinculin-mCherry and: talin-mCherry, GFP-IpaA VBS3, A495K or K498E variants.

(A) Representative confocal micrographs. Scale bar = 5 μm.

(B, D) Distribution of the distance relative to the cell body (d) of filopodial clusters labeled with the indicated marker in cells co transfected with: GFP-talin and vinculin-mCherry (B); VBS3 or vD1 and vincuiin-mCherry (D). Median ± MAD: talin: 2.48 ± 1.81 (858 clusters, N = 3); vinculin: 1.71 ± 1.31 (252 clusters, N = 3); VBS3: 3.08 ± 2.22 (1008 clusters, N = 3); vD1: 2.53 ± 1.79 (537 clusters, N = 3). Mann-Whitney test. **: $p < 0.01$. ****: $p < 0.001$.

(C) Distribution of the distance relative to the cell body (d_c) of filopodial clusters co-labeled with the indicated markers in co-transfected cells. Median ± MAD: VBS3+talin: 2.86 ± 1.49 (285 clusters, N =3); VBS3+vinculin: 1.43 ± 0.88 (128 clusters, N = 3); talin+vinculin: 2.32 ± 1.36 (209 clusters, N = 3). Dunn's test. *: $p < 0.05$. ***: $p < 0.005$. ****: $p < 0.001$.

(E) Percent of filopodia showing VBS3 clusters. VBS3 (563 filopodia, N = 3); A495K (375 filopodia, N = 3); K498E (332 filopodia, N = 3); GFP (495 filopodia, N=3). Pearson's χ^2 test. ****: $p < 0.001$

(F) Dot plot of filopodial lengths. Bar: median ± MAD. VBS3: 34.5 ± 3.6 μm (656 filopodia, N = 4); talin: 24.1 ± 4.4 μm (435 filopodia, N = 4); vD1: 21.0 ± 3.6 μm (336 filopodia, N = 3); A495K: 2.6 ± 0.9 μm (345 filopodia, N = 3); K498E: 2.9 ± 1 μm (434 filopodia, N = 3); GFP+Talin: 3.04 ± 0.01 μm (589 filopodia, N=3); GFP+Vinculin: 2.96 ± 0.01 μm (516 filopodia, N=3); Dunn's test. **: $p < 0.01$. ***: $p < 0.005$. ****: $p < 0.001$.

Figure 6. IpaA VBS3 stabilizes *Shigella*-induced cell adhesions

(A) Representative micrographs of bacterial capture by filopodia. Cells co-transfected with IpaA-VBS3 and talin-mCherry and challenged prior to bacterial challenge. Green IpaA VBS3; red: talin; blue: bacteria; cyan: F-actin. Scale bar = 5 μm. Talin and GFP-IpaA VBS3 are detected at the filopodial tip where bacterial capture occurs, as well as in bacterial coats in invasion foci induced by WT *Shigella* but not the *ipaA* mutant.

(B) Cells were challenged with *ipaA* mutant complemented with: full-length IpaA (1739 cells, N = 5); ΔVBS3: IpaAΔVBS3 (1258 cells, N = 2); ΔVBS1-2: IpaA ΔVBS1-2 (1728 cells, N = 5); A495K: IpaAΔVBS1-2 A495K (1316 cells, N = 4); K498E: IpaAΔVBS1-2 K498E (1291 cells, N = 4); ΔVBSs: IpaA ΔVBS1-3 (909 cells, N = 2). The number of bacteria associated with filopodia per cell was scored. Mann-Whitney test. ****: $p < 0.001$.

(C) HeLa cells were challenged with bacteria for 30 min at 37°C, fixed and processed for immunofluorescence staining. Representative micrographs. Red: bacteria; green: talin. Scale bar = 5 μm.

(D, E) FAs were scored using automatic detection (Exp. Procedures). The median adhesion size (B) and median number per cell (C) are indicated for each sample. (B) Median ± MAD: IpaA: 0.4949 ± 0.3535 (81 cells, N=3); ΔVBS1-2 0.4242 ± 0.2828 (60 cells, N=3); A495K 0.3535 ± 0.3535 (70 cells, N=3); K498E 0.4242 ± 0.2828 (75 cells, N=3); 2.1 0.3535 ± 0.2121 (111 cells N=3); Not Infected: 1.7742 ± 0.5914 (80 cells, N=3). (C) Median ± MAD: IpaA: 17 ± 11 (81 cells, N=3); ΔVBS1-2 29 ± 19 (60 cells, N=3); A495K 5 ± 5 (70 cells, N=3); K498E 23 ± 16 (75 cells, N=3); 2.1 5 ± 4 (111 cells N=3); Not Infected: 29 ± 8 (80 cells, N=3). . (B) Kolmogorov- Smirnov test of probability distribution: *: $p < 0.05$; ****: $p < 0.001$. (C) Kruskal-Wallis: **: $p < 0.01$; ****: $p < 0.001$.

(F) The median size of FAs is plotted for each cell as a function of the adhesions' number per cell.

Table 1 – Non-linear fit values for ITC measurements.

The affinity of synthetic peptides corresponding to talin VBS6, VBS9, VBS33, VBS36, VBS46 and VBS50 for talin H1-H4. Talin VBSs could be divided in four classes according to their affinity for talin H1-H4: while VBS33 and VBS36 did not show detectable binding, VBS6, VBS50 and VBS9 showed weak or moderate affinity for talin H1-H4. Talin VBS46, however, interacted with talin H1-H4 with an affinity comparable to that of IpaA VBS3, with an estimated $K_D = 60 \pm 0.8$ nM. While consistently displaying high affinity for vD1, IpaA and talin VBSs bound to talin H1-H4 with a broad range of K_D values. N (stoichiometry), K_D (affinity constant), ΔH (cal/mol) enthalpy, $-T\Delta S$ (cal/mol) entropic contribution and ΔG (cal/mol) free enthalpy. IpaA VBS3 and talin H46 binding to talin H1-H4 is exothermic ($\Delta G<0$) and mainly driven by enthalpy ($\Delta H<0$ and $\Delta H<-T\Delta S$). Talin H1-H4 binding to IpaA peptides VBS_1 and VBS3 show an important enthalpic and minor entropic contribution. Talin H1-H4 binding to Talin VBS's shows an important enthalpic contribution and an unfavorable entropic contribution to ΔG. The estimated K_D of other talin VBSs for vinculin D1 (K_D vD1) was inferred from previous studies (Izard et al., 2006; Izard and Vonrhein, 2004; Park et al., 2011; Yogesha et al., 2012).

STAR Methods

CONTACT FOR REAGENT AND RESOURCE SHARING

Further information and requests for resources and reagents should be directed to and will be fulfilled by the Lead Contact, Guy Tran van Nhieu (guy.tran-van-nhieu@college-de-france.fr)

EXPERIMENTAL MODEL AND SUBJECT DETAILS

Cell lines

HeLa cells (ATCC CCL-2) were incubated in RPMI (Roswell Park Memorial Institute) medium containing 5% FCS (fetal calf serum, Gibco®) in an incubator with 5% CO_2. Mouse Embryo Fibroblast (MEF) cells were incubated in DMEM (11965092, GIBCO) medium containing 10% FCS (fetal calf serum, Gibco®) in an incubator with 5% CO_2.

Bacterial strains

The wild type *Shigella flexneri*, isogenic mutants, and complemented *ipaA* mutant strains, as well as wild type *Shigella* expressing the AfaE adhesin were previously described (Park et al., 2011). Bacterial strains were cultured in trypticase soy broth (TCS) medium at 37°C. When specified, antibiotics were added at the following concentrations: carbenicillin 100 µg/ml, kanamycin 20 µg/ml.

METHOD DETAILS

Antibodies

The anti-*Shigella* serotype V LPS rabbit antibody was described previously (Tran Van Nhieu et al., 1997)]. The mouse monoclonal anti-talin clone 8d4 antibody was from Sigma-Aldrich. Alexa 405 coupled anti-rabbit and Alexa 488 coupled anti-mouse IgGs were from Jackson Immunoresearch. Alexa 647-coupled phalloidin was from Invitrogen.

Generation of expression constructs.

Full-length human vinculin-mCherry (residues 1-1066) was generated by polymerase chain reaction using 5'- CTGTCGACTGATGCCAGTGTTTCATACG-3' / 5'-CTCCCGGGTCTGGTACCAGGGAGTCTTTC-3' primers and cloned into the pmCherry-N1 (Clontech) vector using the *SalI* - *SmaI* sites. Human talin-mCherry was from Addgene. Human talin-GFP was a gift from K. Yamada. The A483 construct was PCR amplified using 5'- GGCGAATTCCCGGAGACACATATTTAACACG -3' / 5'-GCCGTCGACTTAATCCTTATTGATATTCT -3' primers and cloned into the *Eco*RI - *Sal*I

sites of pGEX-4T-2 (GE Lifesciences). The GFP-A483 plasmid was generated by PCR amplification using the 5'-GCGATATCATGGCCAGCAAAGG-3' and 5'-GCGCGGCCGCTTAATCCTTATTGATATTC-3' primers and cloned into a pcDNA3.1 NT-GFP Topo (Invitrogen). The GFP-IpaAVBS3 plasmid was generated by PCR amplification using the 5'-ACCCGGGGATTAAGCGGCC-3' and 5'-ACCCGGGATCCTGATTTAGTTCC-3' primers and the GFP-A483 plasmid as matrix. The amplicon was digested with *SmaI* and ligated using a T4 DNA Ligase. Mutagenesis to generate the GFP-IpaA VBS3 A495K and K498E variants was performed using the following pairs of primers 5'-CACGGGAAACGATATTTGAAAAATCAAAAAAAGTAACAAACTC-3'; 5'-GAGTTTGTTACTTTTTTTGATTTTTCAAATATCGTTTCCCGTG-3', and 5'-CGATATTTGAAGCTTCAAAAGAAGTAACAACAAACTCCCTAA-3' and 5'-TTAGGGAGTTTGTTGTTACTTCTTTTGAAGCTTCAAATATCG-3', respectively, using the Quickchange II site-directed mutagenesis procedure (Stratagene). All other enzymes were from New England Biolabs. Plasmids containing talin VBS1 (H1-H4) residues 482-636 and GST-IpaA 524-633, as well as peptides IpaA-VBS1 (611-633) and VBS2 (565-586) were previously described (Izard et al., 2006; Papagrigoriou et al., 2004; Ramarao et al., 2007; Tran Van Nhieu and Izard, 2007). IpaA VBS3 (N-TRETIFEASKKVTNSLSNLISLIGT-C, 488-512), and VBS3 variant peptides K9498A (N-TRETIFEASKAVTNSLSNLISLIGT-C), K498E (N- TRETIFEASKEVTNSLSNLISLIGT-C), R489A K498A (N-TAETIFEASKAVTNSLSNLISLIGT-C) and A495K (N-TRETIFEKSKKVTNSLSNLISLIGT-C) were synthetized by Genscript USA Inc. Talin peptides VBS46 (N-YTKKELIECARRVSEKVSHVLAALQ-C, 1945-1970), Talin VBS6 (N-FQDVLMQLANAVASAAAALVLKAKS-C, 664-689), Talin VBS9 (N-RGVGAAATAVTQALNELLQHVKAH-C, 765-789), Talin (N-NLKSQLAAAARAVTDSINQLITMCT-C, 1330-1357) and Talin VBS50 (N-QVVLINAVKDVAKALGDLISATKAA-C, 2077-2102) were synthesized at the Scripps Institute proteomics facility (Jupiter Florida, USA). For crystallographic studies, the human talin H1-H4 domain (residues 481-636) preceded by an internal ribosome-binding site and a start codon was PCR-amplified and cloned into the *EcoRI*/SacI sites of pET28a-IpaA-VBS3 (Park et al., 2011) using the following pairs of primers 5-CGAATTCAGGAGGACAGCTATGCACCGAGGACACATG-3 and 5-CGAGCTCGTTACTGACGGGGCTCAGCACTG-3 to generate the bicistronic expression vector pET28a-IpaA-VBS3/VTBS-talinH1-H4. Plasmids were transformed into the *E. coli* BL21 (DE3) strain (Invitrogen).

Yeast double hybrid analysis.

The yeast two-hybrid analysis was performed using IpaA1-565 as bait to screen a human placental RP1 library, according to standard procedures and the Y2H protocole (Hybrigenics services).

Protein purification.

The talin H1-H4 derivative was purified by affinity chromatography in 25 mM Tris–HCl pH 7.4, 0.5 M NaCl and 30 mM imidazole using a HisTrap HP 5ml affinity column (GE Healthcare). For crystallographic studies, the binary complex of IpaA-VBS3 / talinH1-H4 was purified by passage over a HisTrap HP 5 ml affinity column (GE Healthcare) in 25 mM Tris–HCl pH 7.4, 0.5 M NaCl and 30 mM imidazole. The elution fractions were pooled and concentrated with a 3 kDa cut-off ultrafiltration unit (Amicon), and the buffer was exchanged to phosphate-buffered saline (PBS) and digested by thrombin digestion. The complex was loaded onto a Superdex 200 size chromatography column and fractions containing IpaA-VBS3 / talinH1-H4 complex concentrated up to 30 mg/ml.

IpaA derivatives were purified by affinity chromatography in PBS (Phosphate Buffer Saline) using a GSTrap HP affinity column (GE Healthcare), cleaved with thrombin to remove the GST moiety, followed by size exclusion chromatography (HiLoad S200, Ge Healthcare). For crystallographic studies, talin H1-H4·IpaA-VBS3 binary complex was purified as described (Park et al., 2011). Protein concentration was determined using the BCA assay (Thermo Scientific). Samples were dialyzed in binding buffer and stored at -80°C at concentrations ranging from 1 to 10 mg/ ml.

Native-PAGE analysis.

Talin H1-H4 and IpaA peptides were incubated in binding buffer (25 mM Tris-HCl PH 7.0, 100 mM NaCl and 1 mM β-Mercaptoethanol) for 1hr at 4°C. After incubation, samples were resuspended in 2 x Native loading buffer (62,5mM Tris pH 6,8 containing 25% Glycerol) and separated by Tris-Glycine Native-PAGE electrophoresis (Schagger et al., 1994). Gels were stained using standard colloidal Coomassie stain.

SEC-MALS

The purified proteins IpaA483-633, IpaA524-633 and talin H1-H4 were used at 20µM equimolar concentrations and incubated at 4°C for one hour in binding buffer (25 mM Tris-HCl PH 7.0, 100 mM NaCl and 1 mM β-Mercaptoethanol). 200µls of the protein mixtures were analyzed by size-exclusion chromatography (SEC) on a Superdex 200 10/300 GL (GE Healthcare) using a Shimadzu Prominence HPLC. Multi-angle laser light scattering (MALS) was measured with a MiniDAWN TREOS equipped with a quasi-elastic light scattering module and a refractometer Optilab T-rEX (Wyatt Technology). Protein concentration was determined using a specific refractive index (dn/dc) of 0.183 at 658 nm.

Crystallization, structure determination, and crystallographic refinement

Crystals of the IpaA-VBS3 / talin H1-H4 complex were obtained by mixing 1 µl of protein complex at 7 mg/ml in buffer 25 mM Tris pH 7.4 and 150 mM NaCl with 1 µl of 0.2 mM ammonium sulfate, 0.1 mM sodium acetate pH 4.6 and 30 % PEG 4000 by vapor diffusion at 292 K. Crystals were cryoprotected with a solution consisting of the reservoir supplemented with 20 % v/v ethylene glycol and flash frozen. X-ray diffraction data were collected at 100 K on a single crystal at PROXIMA-1 beamline at the SOLEIL synchrotron (Saint-Aubin, France). Data were indexed and processed using XDS (Kabsch et al., 2010) and corrected for anisotropy with the STARANISO server (staraniso.globalphasing.org). Structure solution was obtained by molecular replacement with Phaser (McCoyet al., 2007) using as search template a monomer of talin-H1-H4 derived from the pdb entry 1sj8 lacking residues 515 to 538. A clear solution was obtained (TFZ = 28.5; LLG = 2105.5) Refinement was done with autoBUSTER (Bricogne et al., 2010) using NCS and alternating with manual building in Coot (Emsley et al., 2010). One TLS group per chain was used at the end of the refinement. Final structure is deposited on ProteinDataBank (PDB ID: 5NL1).

Isothermal titration calorimetry.

Protein interaction was analyzed by microcalorimetry using an ITC200 calorimeter (MicroCal) at 25°C. 200 µls of 20-100 µM of talin H1-H4 protein in binding buffer (25 mM Tris-HCl pH 7.0, 100 mM NaCl and 1 mM β-mercaptoethanol) were added to the cell and binding was measured in the presence of different concentrations of IpaA / talin VBSs peptides. In other experiments, A483 or A524 were added to the cell and binding of talin H1-H4 (100 µM) was measured. Typically 20-40 injections of 2 µls of ligand were made with intervals of

320 seconds between each addition, with a reference power of 12 µcal / sec. Data was analyzed using the MicroCal software provided by manufacturer.

siRNA transfection

HeLa cells were seeded at a density of 10^5 cells in wells containing a 22 x 22 mm coverslip in a 6-well plate. The following day, cells were transfected with of anti-talin 1 siRNA (Stealth Select RNAi, catalogue no. 1299003, Invitrogen, oligo 804; sequence: 5′-CCAAGAACGGAAACCUGCCAGAGUU-3') or anti-vinculin siRNA (Stealth Select RNAi, catalogue no. 1299001, Invitrogen, oligo VCLH55111259) duplex at the indicated concentrations and time periods.

Cell challenge with *Shigella* strains

HeLa cells seeded at 2 x 10^5 cells in coverslip-containing 33 mm-diameter wells the day before, were transfected with the indicated constructs using the JetPei® transfection reagent. After 16 hours, cells were challenged with *Shigella* strains coated with poly-L-lysine, as follows. Bacteria grown to an $OD_{600\ nm}$ of 0.6 - 0.8 were washed three-times by successive centrifugation at 13 Kg for 30 sec and resuspension in EM buffer (120 mM NaCl, 7 mM KCl, 1.8 mM $CaCl_2$, 0.8 mM $MgCl_2$, 5 mM glucose, and 25 mM HEPES, pH = 7.3). Samples were resuspended in EM buffer containing 50 µg/ml poly-L-lysine and incubated for 15 min at 21°C, washed three times in EM bufer and resuspended in the same buffer at a final OD of $OD_{600\ nm}$ = 0.2. Cell samples were washed three times in EM buffer and challenged with 1 ml of the bacterial suspension and incubated at 37°C. Samples were fixed with PBS containing 3.7% PFA after 15 min incubation for the analysis of filopodial capture. Alternatively, for the analysis of focal adhesions in infected cells, a similar procedure was used except that cells were seeded at a density of 400 000 cells / well and challenged after 16H for 60 min with poly-L-lysine coated bacteria prior to fixation with a 1:1 ethanol-acetone solution for 5 min at -20°C. Samples were processed for immunofluoresence microscopy.

Immunofluorescence microscopy analysis

For GFP-IpaA VBS3, GFP and talin / vinculin co-localization experiments MEF cells were seeded at a density of 1 x 10^4 cells in a µ-Dish 35 mm 15 kPa stiffness chamber (Cat #81391, ibidi) coated with 10 µg / ml of Fibronectin (Calbiochem). Cells were transfected with plasmids encoding human talin-mCherry, vinculin-mCherry, GFP-IpaA VBS3 and GFP using the Lipofectamine 2000 transfection reagent (Life Technologies). For replating experiments HeLa cells co-transfected with vinculin-mCherry and talin-GFP, were resuspended by trypsinization

and replated on glass coverslips. After 20 minutes the samples were fixed, processed for immunofluorescence microscopy, and mounted on slides using Dako mounting medium (Dako, Agilent Technologies), as described (Romero et al., 2012).

Samples were analyzed using an Eclipse Ti microscope (Nikon) equipped with a 100x objective, a CSU-X1 spinning disk confocal head (Yokogawa), and a Coolsnap HQ2 camera (Roper Scientific Instruments), controlled by the Metamorph 7.7 software. The percent of internalized bacteria was scored as one if the number of internalized bacteria per foci was at least the 50% of the total number of bacteria in the foci or zero if below, in three independent experiments ($n_{control}$=27, $n_{siRNATln}$=23). For control and anti-talin siRNA transfected cells, the percent of internalized bacteria was compared using a Chi-Squared test (R Statistical Software).

Image processing and analysis

Analysis was performed in Icy Bioimaging Analysis software (de Chaumont et al., 2012). Scans of GFP-IpaA VBS3, Vinculin-mCherry and Talin-mCherry were performed as follows. Defined ROIs in median projections of basal in-focus planes were segmented in concentric areas from the edge of the cell. Average values of intensities were normalized to the maximum and minimum average intensities of the ROI. For talin-GFP and vinculin-mCherry filopodial distribution, saturated sum projections of images from 20 minutes-replated cells were used for Concentric Area Scan analysis. For the quantification of the number of FAs, a semi-automated protocol was developed using Icy software (de Chaumont et al., 2012). Spinning-disk fluorescent microscopy planes were used to detect GFP-IpaA VBS3 structures using HK means thresholding and overlaid binary masks obtained from the threshold projections of F-actin labeled images (Max-entropy method). FAs were detected as spots positive for both GFP- IpaA VBS3 and actin structures using Wavelet Spot Detector. FAs were detected as spots positive for both GFP- IpaA VBS3 above background intensity levels. Filopodia length and number were determined manually from actin-labeled projections. IpaA VBS3, talin, vinculin and vD1 filopodial clusters were identified using Wavelet Spot Detector in Saturated sum projections. Co-localizing clusters were determined by overlaying the separate detections. Distance to cell body was determined using ROI Inclusion analysis plugin.

QUANTIFICATION AND STATISTICAL ANALYSIS.

Bacterial internalization and talin coat-structure formation were analyzed a contingency table using in a Pearson Chi-Squared test (R Statistical Software). A Post-hoc pairwise Chi-square test (NCStats package, R Statistical Software) with FDR p-value correction was further

used to compare the distribution between the various strains. n > 35 foci, N = 3. The correlation of the intensity of talin and vinculin labeling was analyzed using a Wilcoxon rank sum test (R Statistical software).

For all statistical tests a D'Agostino-Pearson normality test was performed in order to decide if performing a parametric or a non-parametric test. Applied statistical test, number of datapoints (n) and number of experimental replicates (N) are indicated in the figure legends; as well as mean ± SEM, for normally-distributed data, and median ± MAD, otherwise.

DATA AND SOFTWARE AVAILABILITY

Crystallographic structure of the IpaA-VBS3 / talin H1-H4 complex was deposited on the Protein Data Bank, with PDB ID: 5NL1.

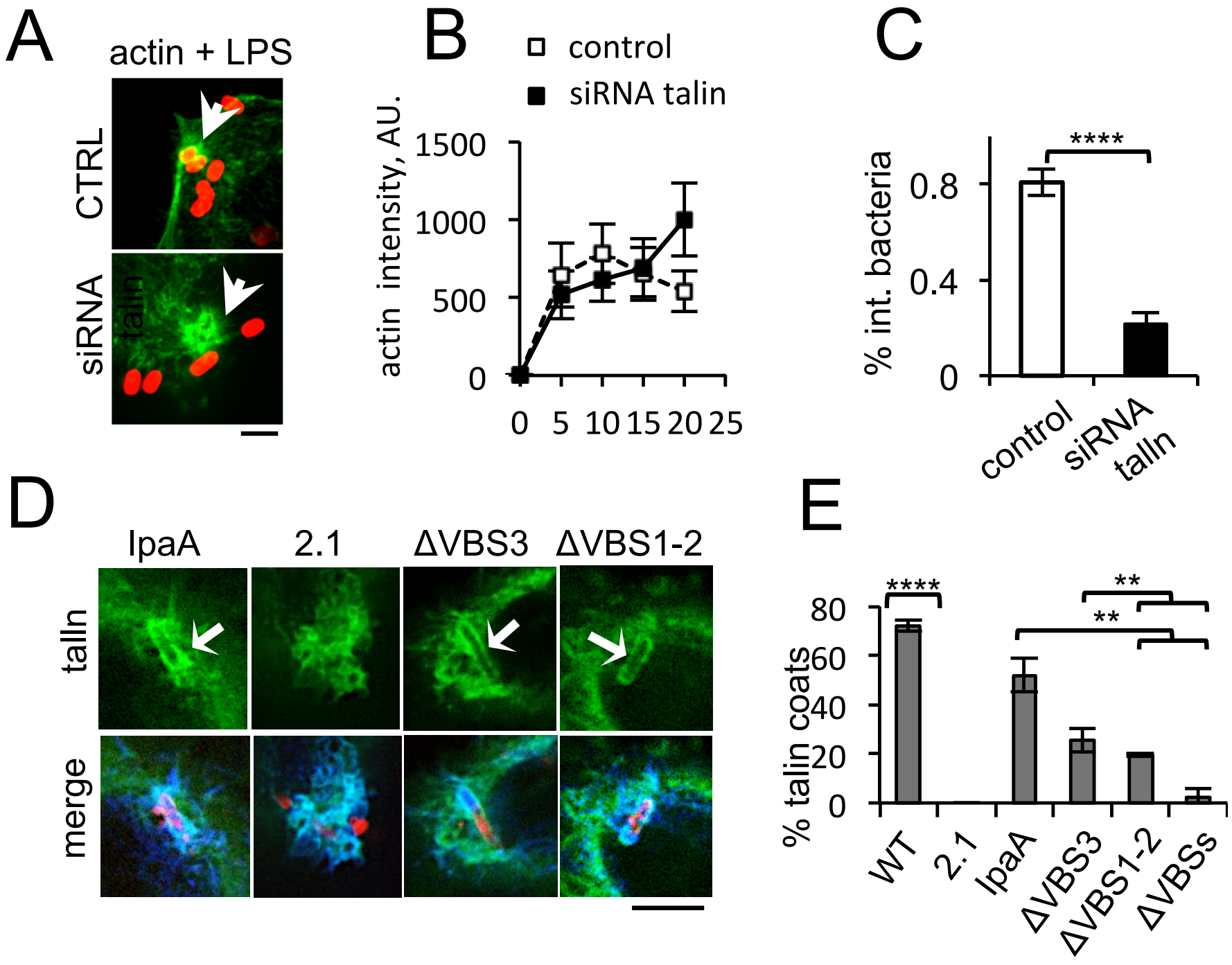
A
actin + LPS
CTRL
siRNA talin
B
control
siRNA talin
actin intensity, AU.
1500
1000
500
0
0 5 10 15 20 25
C
****
% int. bacteria
0.8
0.4
0
control
siRNA talin
D
IpaA
2.1
ΔVBS3
ΔVBS1-2
talin
merge
E
****
**
**
% talin coats
80
60
40
20
0
WT
2.1
IpaA
ΔVBS3
ΔVBS1-2
ΔVBSs

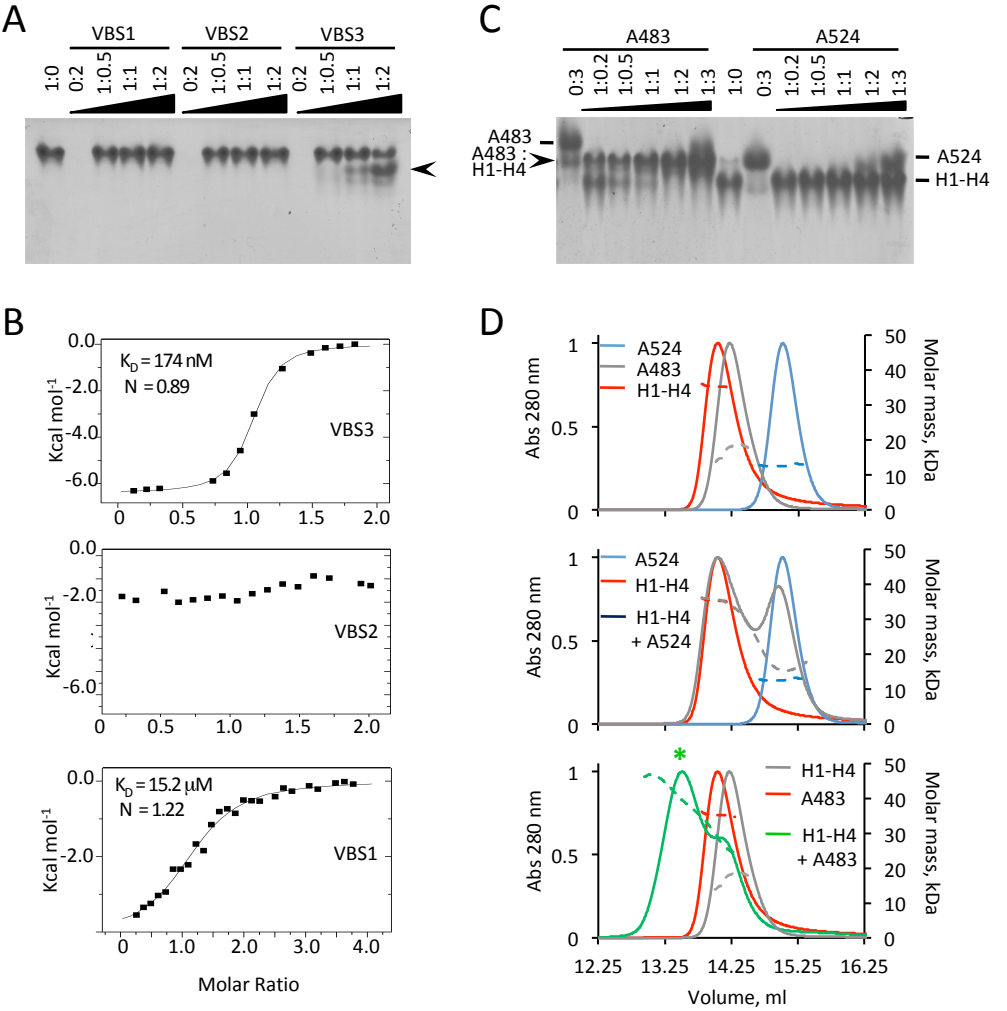
A
VBS1
VBS2
VBS3
1:0
0:2
1:0.5
1:1
1:2
C
A483
A524
0:3
1:0.2
1:0.5
1:1
1:2
1:3
1:0
A483
A483 :
H1-H4
A524
H1-H4
B
K_D = 174 nM
N = 0.89
VBS3
K_D = 15.2 µM
N = 1.22
VBS1
VBS2
Kcal mol^{-1}
Molar Ratio
D
A524
A483
H1-H4
H1-H4
+ A524
H1-H4
+ A483
Abs 280 nm
Molar mass, kDa
Volume, ml

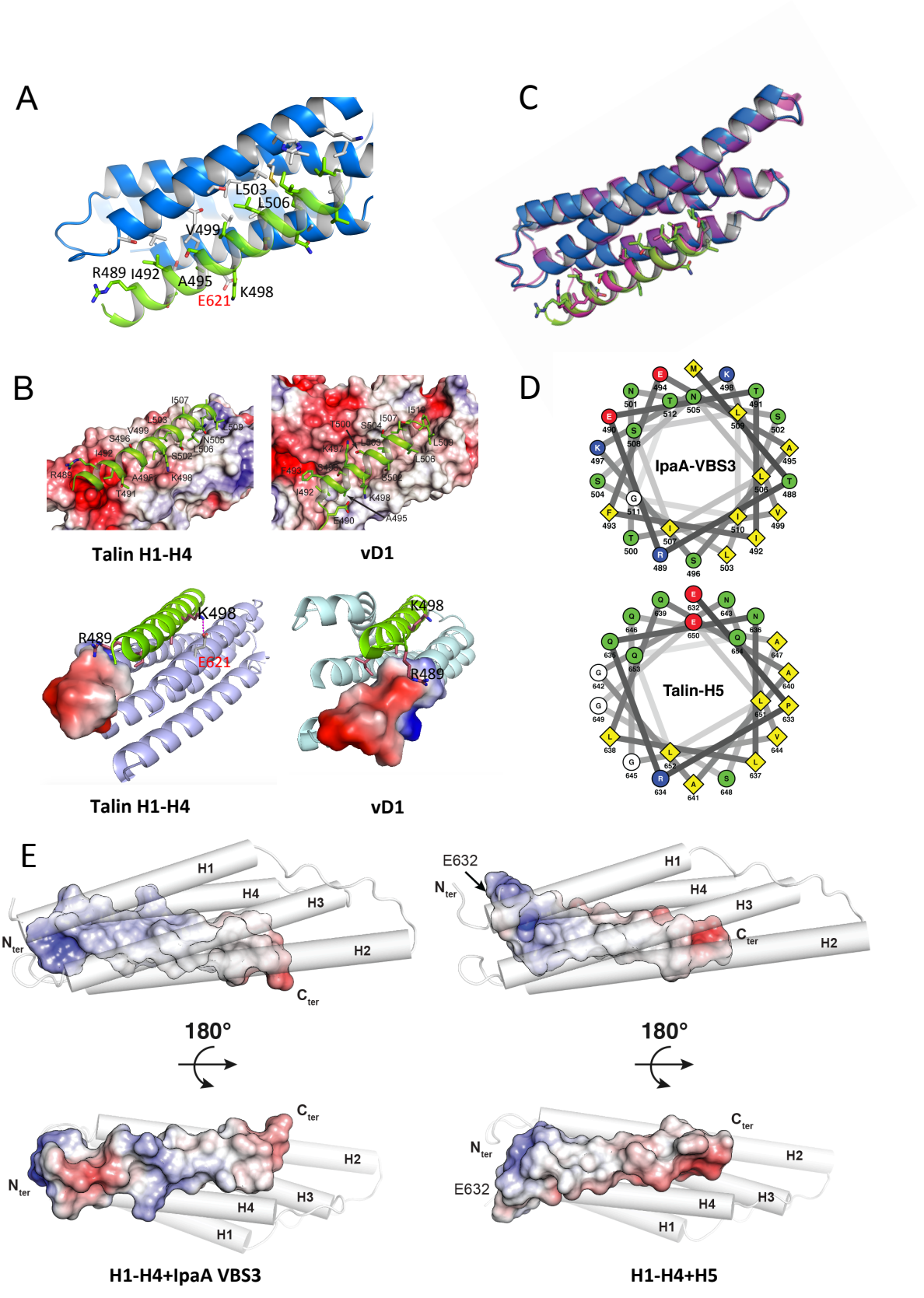

Fig. 3. IpaA VTBS interacts with talin and vinculin via different mechanisms

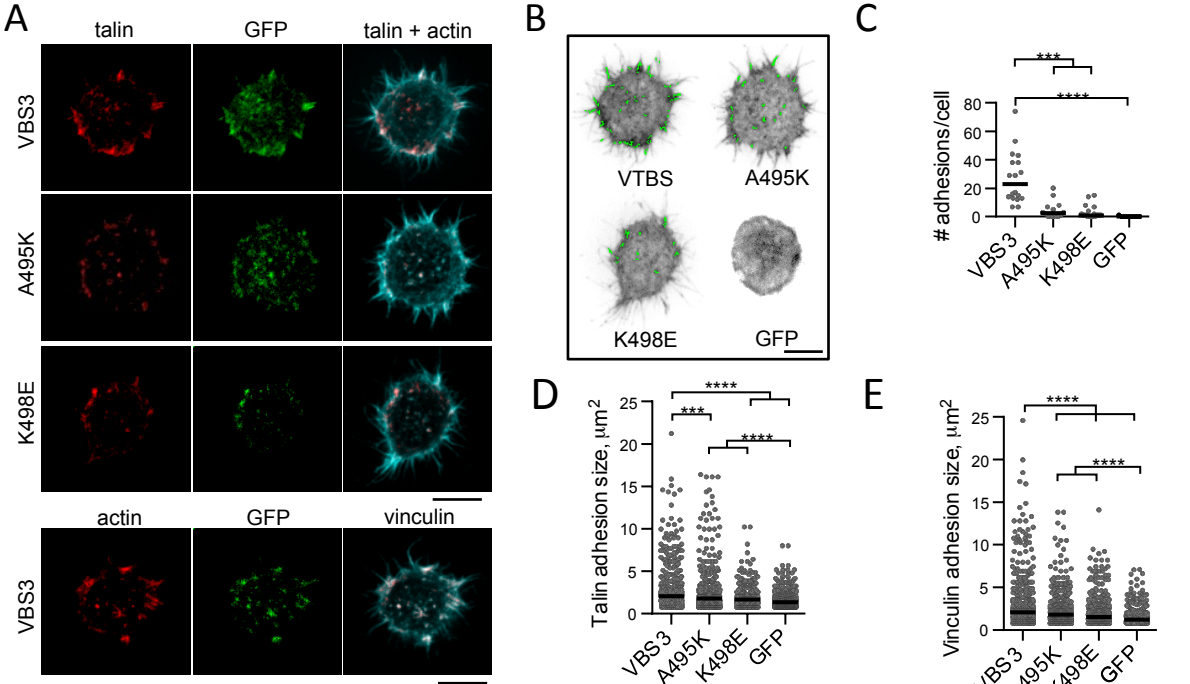
A
talin
GFP
talin + actin
VBS3
A495K
K498E
actin
GFP
vinculin
VBS3
B
VTBS
A495K
K498E
GFP
C
adhesions/cell
80
60
40
20
0
***
****
VBS3
A495K
K498E
GFP
D
Talin adhesion size, µm2
25
20
15
10
5
0
****
***
****
VBS3
A495K
K498E
GFP
E
Vinculin adhesion size, µm2
25
20
15
10
5
0
****
****
VBS3
A495K
K498E
GFP

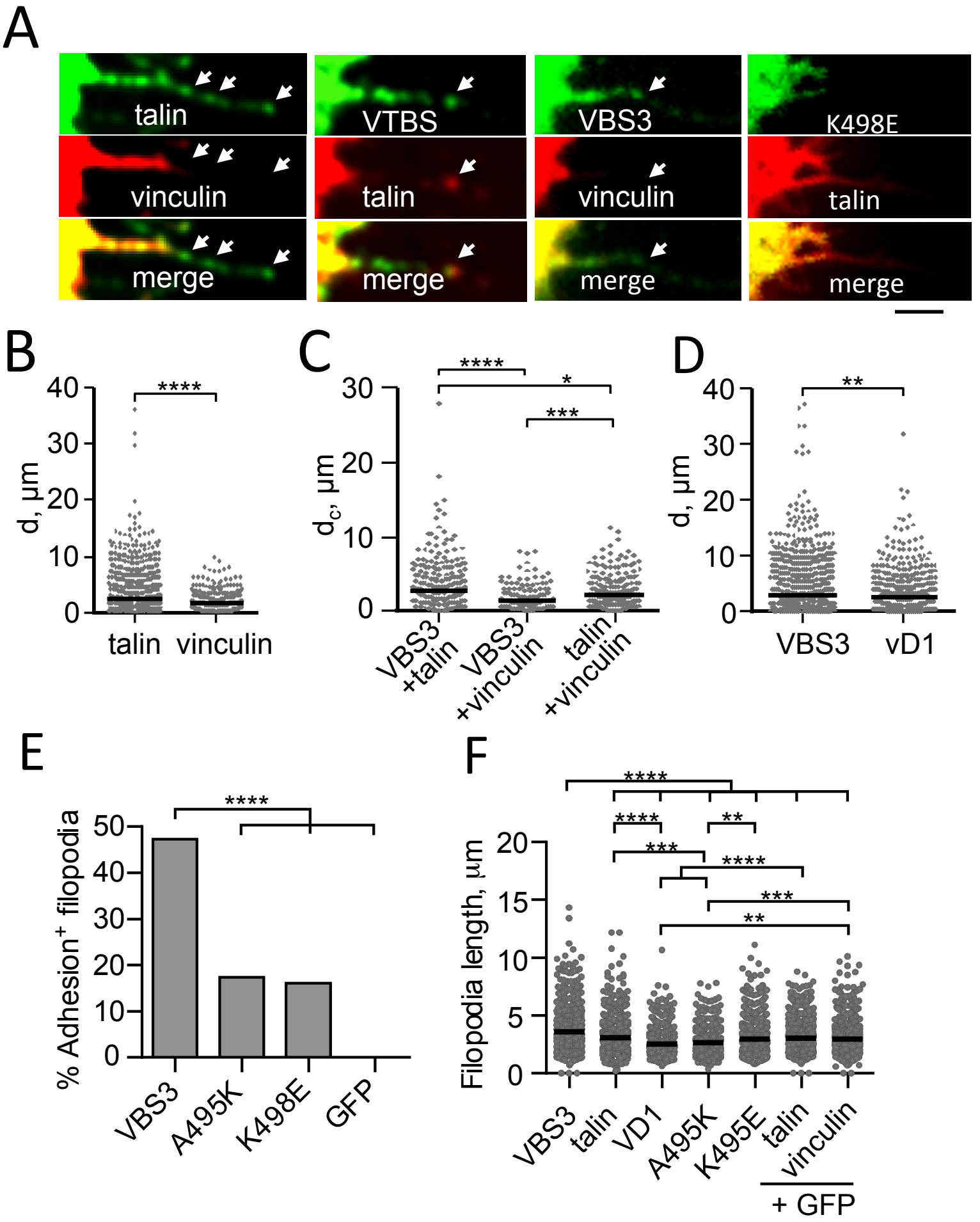
A
talin
vinculin
merge
VTBS
talin
merge
VBS3
vinculin
merge
K498E
talin
merge
B
d, µm
****
talin
vinculin
C
d_c, µm
****
*
***
VBS3 +talin
VBS3 +vinculin
talin +vinculin
D
d, µm
**
VBS3
vD1
E
% Adhesion+ filopodia
****
VBS3
A495K
K498E
GFP
F
Filopodia length, µm
****
****
**
***
****
***
**
VBS3
talin
VD1
A495K
K495E
talin
vinculin
+ GFP

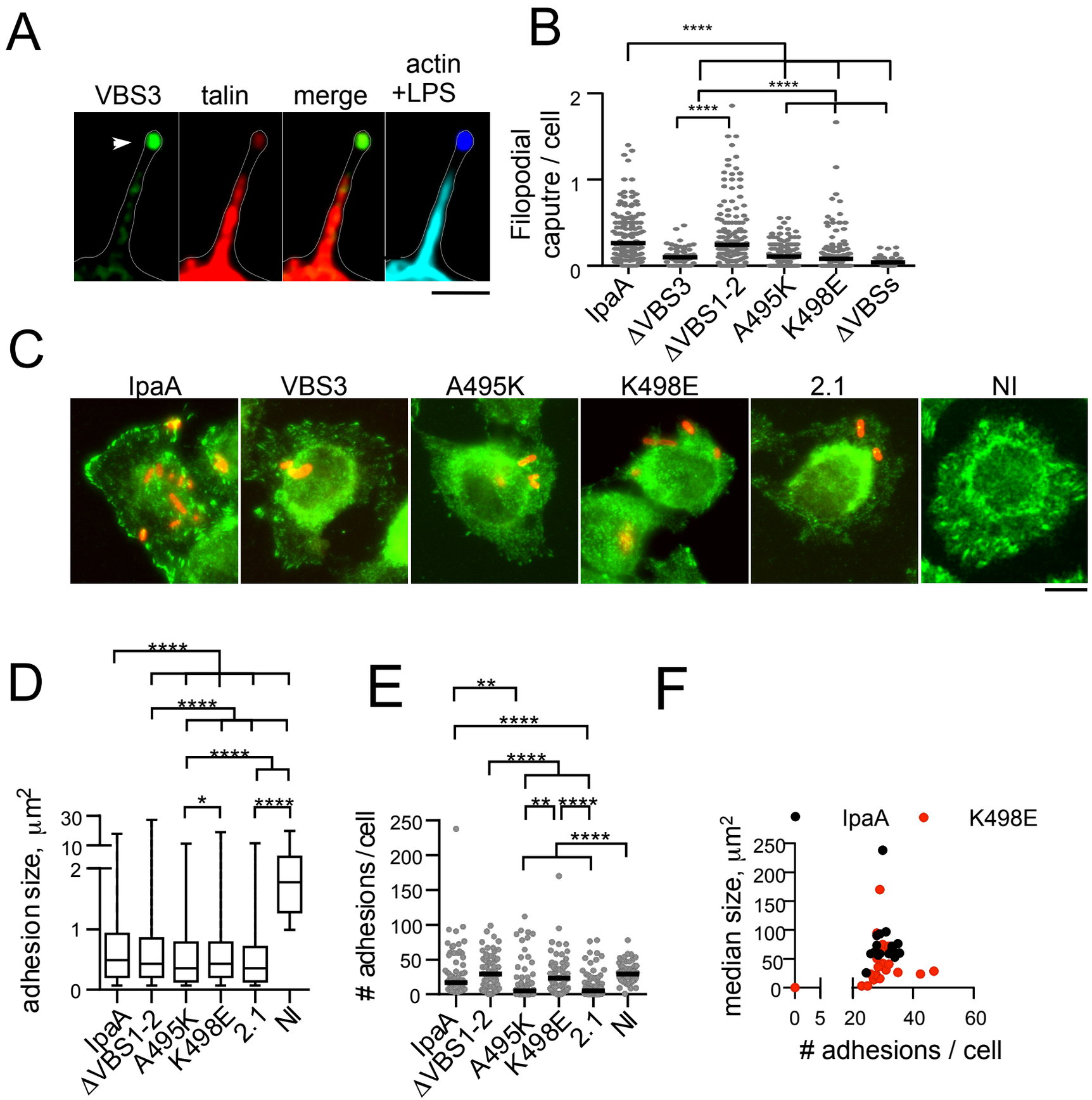
A
VBS3
talin
merge
actin
+LPS
B
Filopodial caputre / cell
IpaA
ΔVBS3
ΔVBS1-2
A495K
K498E
ΔVBSs
C
IpaA
VBS3
A495K
K498E
2.1
NI
D
adhesion size, µm²
E
adhesions / cell
F
median size, µm²
adhesions / cell
IpaA
K498E

Cell	Titrant	K_D (Talin H1-H4)	N	DH (Kcal/mol)	-TDS (Kcal/mol)	DG (Kcal/mol)	K_D (vD1)
Talin H1-H4	**IpaA VBS1**	15.2 ± 1.1 µM	1.22	-4.10	-2.47	-6.57	110 pM
	IpaA VBS2	-	-	-	-	-	6.6 nM
	IpaA VBS3	174.5 ± 18.9 nM	0.89	-6.65	-2.81	-9.47	54 pM
	IpaA VBS3 K498A	163.1 ± 1.1 nM	1.18	-6.28	-2.97	-9.26	n.d.
	IpaA VBS3 K498E	300.3 ± 2.8 nM	0.73	-12.1	3.25	-8.90	n.d.
	IpaA VBS3 R489A K498A	328.9 ± 1.9 nM	0.69	-8.68	-0.16	-8.84	n.d.
	IpaA VBS3 A495K	2.93 ± 0.2 µM	1.05	-3.73	-3.81	-7.54	n.d.
	Talin VBS46	60 ± 0.8 nM	0.92	-16.97	7.20	-9.77	3 nM
	Talin VBS6	21 ± 3.4 µM	1.26	-14.34	7.97	-6,37	n.d.
	Talin VBS9	1 ± 0.1 µM	1.29	-14.65	6.47	-8,18	n.d.
	Talin VBS50	45 ± 7.5 µM	1.02	-13.23	7.31	-5,92	99 nM
	Talin VBS33	No binding	-	-	-	-	n.d.
	Talin VBS36	No binding	-	-	-	-	n.d.
A483 (Site 1)	**Talin H1-H4**	115.7 ± 32.15 nM	1	-6.38	-3.07	-9.45	n.d.
A483 (Site 2)		4.6 ± 0.6 µM	1	-6.76	-5.01	-7.27	n.d.
A524 (Sites 1 + 2)		2.0 ± 0.5 µM	1.52	-3.97	-3.78	-7.76	n.d.

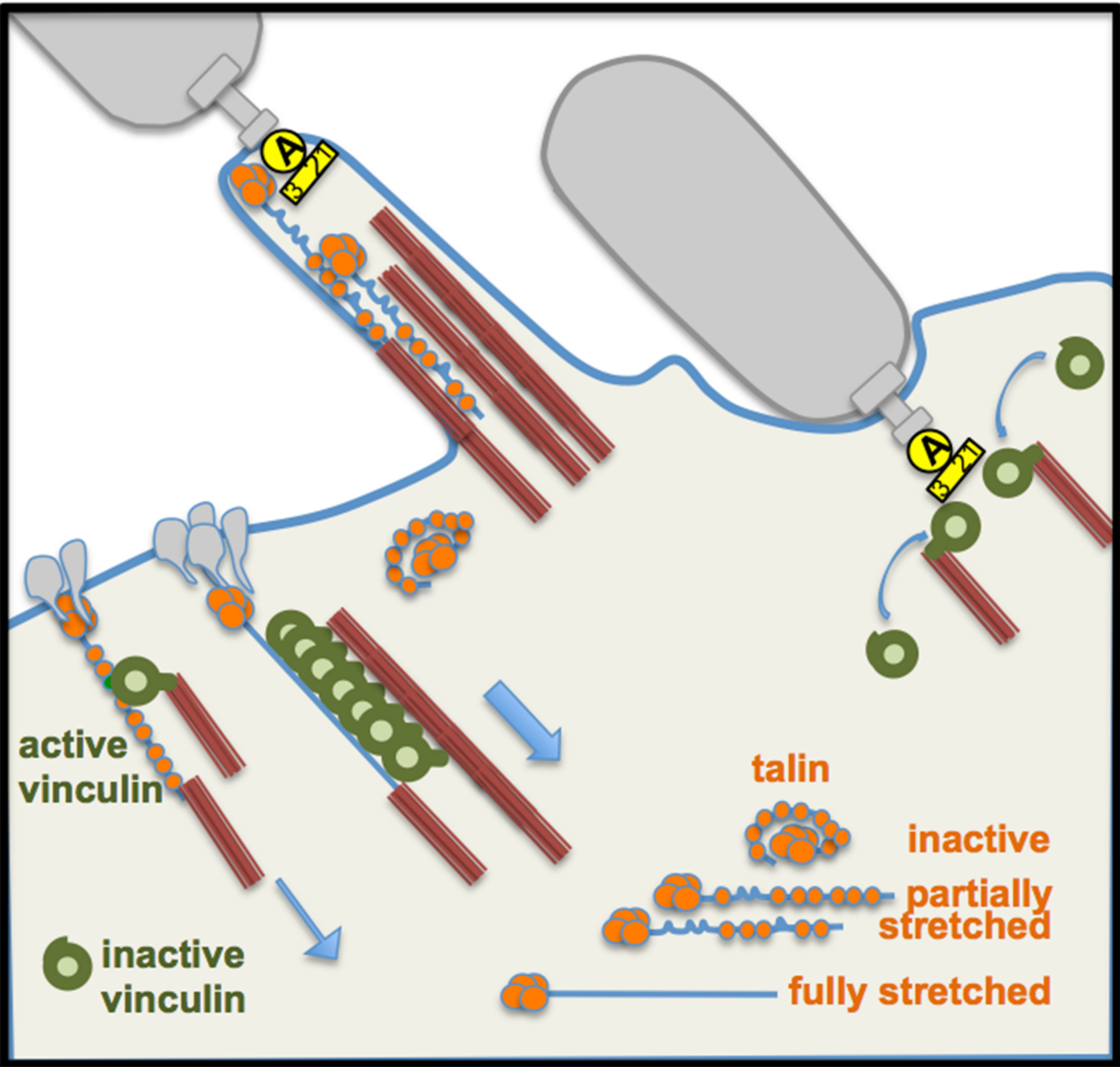
A
β21
A
β21
active
vinculin
inactive
vinculin
talin
inactive
partially
stretched
fully stretched